Compact and Low Loss silicon-integrated polarization beam splitter developed by efficient semi-inverse design approach

Yuqi Zhao[1], Jingshu Guo[1,2*], Laiwen Yu[1], Guojiang Yang[1], Chenxu Zhou[1], Tianyu Cao[1], Daoxin Dai[1,2,3]

[1] *College of Optical Science and Engineering, State Key Laboratory for Modern Optical Instrumentation, International Research Center for Advanced Photonics, Zhejiang University, Zijingang Campus, Hangzhou, 310058, China.*

[2]*Jiaxing Key Laboratory of Photonic Sensing & Intelligent Imaging, Intelligent Optics & Photonics Research Center, Jiaxing Research Institute Zhejiang University, Jiaxing 314000, China.*

[3]*Ningbo Research Institute, Zhejiang University, Ningbo 315100, China.*

[*]Corresponding Author: E-mail: jsguo@zju.edu.cn

***Abstract*—We demonstrate a low loss silicon-integrated polarization beam splitter with by using an efficient semi-inverse design approach. It has more compact footprint with decent performance when compared to the state-of-the-art counterparts designed by conventional methods.**

Keywords—silicon photonics, polarization beam splitter, inverse design, subwavelength gratings

I. INTRODUCTION

The polarization beam splitter (PBS) is an important fundamental polarization-handling device that can combine/separate the TE mode and the TM mode in waveguides [1]. It is needed in various applications, such as optical communication systems, laser systems, and scientific instrumentation.

Currently, the PBSs based on conventional design methods have been demonstrated with high performances [2-3]. Nevertheless, it is still desired to shrink the device footprint. In this paper, with our previous semi-inverse design methods, we realize a PBS with ultra-compact footprints of 1.6×4.9 μm^2 and decent performance comparable to the state-of-the-art counterparts developed by the classical forward design approaches.

II. METHODS AND SIMULATION

To achieve a high-efficiency inverse design, it is important to minimize the search space dimension while ensuring that the final design is optimal. In our previous work, we proposed an efficient inverse design method that utilizes a multi-stage optimization iteration strategy with manual interventions [4]. The geometry definition strategy that we used can support flexible adjustment of the search-space dimension, while the manual interventions, such as structure interpolation and extension, EM solver adjustment, and mesh accuracy change, help to ensure that the inverse design with the multi-stage optimization strategy has the potential to produce high-performance functional photonic devices with limited computation cost.

The design parameters are defined similarly to our previous work [5]. As Fig. 1(a) shows, the 3D schematic diagram for the final designed device. Moreover, Fig.1(b) explains the specific meaning of the parameters in detail by the top view. The device is divided into n sections along the lengthwise direction, with each section having a length defined as $\boldsymbol{L} = [l_1, l_2, \ldots, l_n]$. The parameters $\boldsymbol{D_n} = [d_{n1}, d_{n2}, \ldots, d_{n12}]$ define the lateral corner location in the y direction at the yz cross-sectional interface between the $(n\text{-}1)$-th and the n-th sections. The metamaterial SWG structure has a period P and a fill factor Λ. The input/output (I/O) waveguides are characterized by the waveguide w_{in} and w_{out}, the positions of Port #1 and Port #3 in the y-axis, d_{in0} and d_{out0}, respectively, and the separation between the adjacent output waveguides, d_{out}. The length of the waveguide taper connecting the optimization region and the input (output) waveguide is denoted by l_{in} (l_{out}). The parameter set $\boldsymbol{S_{total}}$ to be optimized can combine flexibly combine any related parameters such as $\boldsymbol{S_{total}}=[\boldsymbol{D_1}, \boldsymbol{D_2}\ldots\boldsymbol{D_n}, \boldsymbol{D_{n+1}}]$ or $\boldsymbol{S_{total}}=[\boldsymbol{D_1}, \boldsymbol{D_2}\ldots\boldsymbol{D_n}, \boldsymbol{D_{n+1}}, \boldsymbol{L}, l_{in}, l_{out}]$.

Assuming modes #1, 3, 5 and #2, 4, 6 are respectively the TE-polarization modes and TM-polarization modes supported by ports #1, 2, 3 (Fig. 1), it is desired to achieve 100% transmissions of TE and TM channels, i.e., $|S_{31}|^2=1$ and $|S_{62}|^2=1$.

The FOM is given by $\mathrm{FOM} = -10log_{10}(|S_{31}|^2 \times |S_{62}|^2) / 2$. Only the center wavelength (1.55 μm) is considered. Since the device is compact enough, we use only a 3D-FDTD solver (with acceptable computational cost). Through the design flow, two mesh configurations were used. In the fast-simulation-mesh, there are 14 mesh points per effective-wavelength scale. The simulation of one sample consisting of two runs of the FDTD solver costs ~18 seconds. In the high-accuracy-mesh, there are 18 mesh points per effective-wavelength scale, and the local mesh refinements were adopted. In this case, the simulation of one sample costs about 2 minutes. The performance confirmation of the final designed device was carried out by the FDTD solver with very dense meshes (26 mesh points per effective-wavelength scale).

The design starts from an initial symmetric Y-branch structure. First, the air-slot device was designed. The optimization region length L is manually set to 2.5 μm at the beginning of the design flow and then changes to 3.4 μm gradually. After a total of 572 generations of iterations, the FOM reaches 0.36 dB. Then a SiO_2-slot device was designed using this result as an initial individual. The design flow includes a total of 42 generations of iterations. The final FOM is 0.335 dB. The geometric parameters of the final device are given in Table 1. The final device has a 34-section optimization region with 35 cross-sections. The SWG period and fill factor are respectively P = 0.2 μm and Λ = 0.5.

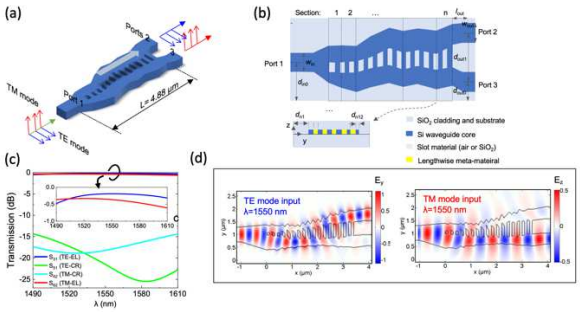

Fig. 1. (a) 3D schematic diagram. For the final designed device. (b) Top view (xy-plane) and cross-sectional view (yz-plane) at the interface between Section *n-1* and Section *n* (c) The simulated optical propagation fields at 1550 nm. (d) The simulated transmissions.

TABLE I. THE DETAILED GEOMETRIC PARAMETERS OF THE FINAL DESIGNED SiO_2-SLOT PBS (UNIT: MICRON)

Optimization Region Parameters in y-direction					Optimization Region Parameters in x-direction		Else parameters	
dmn	*n*							
	1	*2*	*3*	*4*				
1	0.417	0.562	0.111	0.303				
2	0.447	0.565	0.092	0.246	l_1	0.1	w_{in}	0.585
3	0.424	0.544	0.166	0.278	l_2	0.2	d_{in}	1.013
4	0.451	0.507	0.122	0.281	l_3	0.3	w_{out}	0.45
5	0.402	0.558	0.13	0.274	l_4	0.4	d_{out0}	0.795
6	0.449	0.488	0.144	0.261	l_5	0.5	d_{out}	1.003
7	0.513	0.5	0.158	0.225	l_6	0.6	l_{in}	0.974
8	0.453	0.441	0.195	0.244	l_7	0.7	l_{out}	0.509
9	0.517	0.46	0.228	0.234	l_8	0.8		
10	0.503	0.335	0.228	0.289	l_9	0.9		
11	0.531	0.419	0.228	0.214	l_{10}	1		
12	0.501	0.364	0.219	0.242	l_{11}	1.1		
13	0.561	0.376	0.281	0.183	l_{12}	1.2		
14	0.537	0.304	0.271	0.22	l_{13}	1.3		
15	0.564	0.413	0.306	0.223	l_{14}	1.4		
16	0.541	0.297	0.297	0.251	l_{15}	1.5		
17	0.604	0.368	0.359	0.221	l_{16}	1.6		
m 18	0.556	0.27	0.31	0.276	l_{17}	1.7		
19	0.594	0.348	0.372	0.27	l_{18}	1.8		
20	0.559	0.287	0.387	0.238	l_{19}	1.9		
21	0.611	0.319	0.445	0.233	l_{20}	2		
22	0.584	0.225	0.44	0.258	l_{21}	2.1		
23	0.617	0.315	0.496	0.323	l_{22}	2.2		
24	0.573	0.264	0.485	0.283	l_{23}	2.3		
25	0.571	0.289	0.549	0.306	l_{24}	2.4		
26	0.572	0.302	0.609	0.348	l_{25}	2.5		
27	0.574	0.296	0.57	0.293	l_{26}	2.6		
28	0.566	0.366	0.5	0.393	l_{27}	2.7		
29	0.529	0.309	0.587	0.351	l_{28}	2.8		
30	0.555	0.374	0.579	0.437	l_{29}	2.9		
31	0.524	0.383	0.569	0.394	l_{30}	3		
32	0.533	0.399	0.544	0.397	l_{31}	3.1		
33	0.524	0.442	0.568	0.399	l_{32}	3.2		
34	0.531	0.452	0.518	0.439	l_{33}	3.3		
35	0.505	0.473	0.525	0.43	l_{34}	3.4		

The designed PBS has an ultra-compact footprint of 1.6×4.9 μm^2. As shown in Figures 1(b) and 1(c), the TE- and TM-polarization modes can respectively output at ports #2 and #3 with low losses. Their ELs are 0.19-0.48 dB and 0.33-0.61 dB in theory, respectively, and the ERs are higher than 13.8 dB in the wavelength range of 1490-1610 nm (Fig. 1b).

III. RESULTS

The experimental PBS device is shown in Fig. 3. The photonic integrated circuit (PIC) has been measured and consists of a pair of TE grating couplers and a pair of TM grating couplers, as shown in Fig.2(a). In addition, a scanning electron microscope (SEM) image of the fabricated device is presented in Fig. 2(b).

The measured transmissions of the fabricated PBSs are shown in Fig. 2(c-d). It can be seen that the measured ER is >14.9 dB in the wavelength range of 1520-1610 nm for the TE polarization mode. Meanwhile, the extinction ratio (ER) for the TM polarization mode is >9.0 dB in the wavelength range of 1520-1561 nm. The relatively low ER may be due to the imperfect fabrication of the fine convex structures. To characterize the ELs (which are too low to be measured precisely), the testing structures with ten and twenty PBSs in cascade are introduced. The ELs measured from the cut-off method [6] are < 0.44 dB and < 0.62 dB in the wavelength range of 1520~1610 nm for TE- and TM-polarization modes, respectively, as shown in Fig. 2(c).

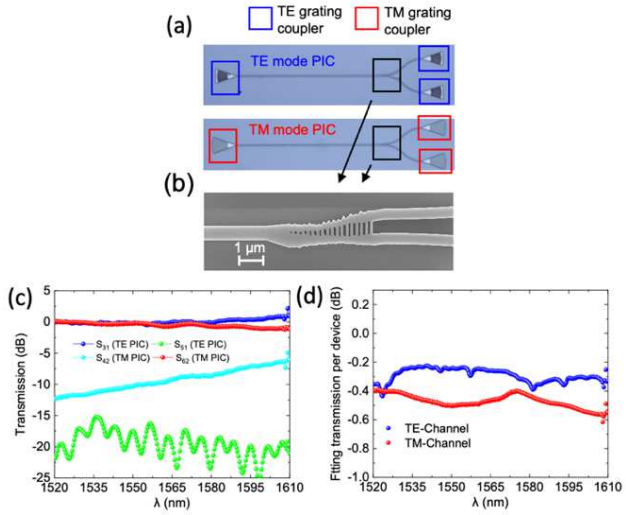

Fig. 2. (a) The microscope pictures of the TE/TM mode measurement PICs. (b) The SEM picture of the fabricated polarization beam splitter. (c) The measured transmissions of a single device. (d) The fitting transmissions per device from cascaded measurements.

The summary for the state-of-the-art silicon PBSs is also given in Table 2. In contrast to the PBSs designed by conventional methods, the present PBS has similar ELs and ultra-compact footprints, while the ER and the bandwidth are slightly inferior. The ER performance can be improved by using cascaded structures, regarding that the present PBS has a low EL (<0.6 dB).

TABLE II. SUMMARY OF THE STATE-OF-THE-ART SILICON PBSS DEVICE ON SILICON

Type, year	Footprint (μm^2)	EL (dB)		ER (dB)		BW (nm)		Ref.
		Sim.	*Exp.*	*Sim.*	*Exp.*	*Sim.*	*Exp.*	
Asymmetric waveguide coupler, 2019	L>11 μm	<0.6	<2	ER>23	ER>20	175	175	[7]
Metamaterial waveguide, 2019	12.25×1.9	<0.9	<1	ER>20	ER>20	>200	>200	[8]
subwavelength-grating waveguides, 2020	L:33.6 μm	<0.3	<1	ER>20	ER>20	>270	~230	[9]
Inverse design (2016)	1.4×1.4	<0.5	<2.1	ER>15	ER>12	>100	120	[10]
Inverse design, 2020	L=>5 μm	<0.4	<0.5	ER>13	ER>16.7	100	75	[11]
Semi-Inverse Design	1.61×4.88	<0.6	<0.6	ER>13.8	ER>9	120	41	This work

a. Abbreviation definitions: EL, excess loss; ER, extinction ratio; BW, bandwidth; Sim., simulated result; Exp., experimental result; PBS, polarization beam splitter.

IV. CONCLUSION

In conclusion, we have successfully applied our semi-inverse design method to the design and production of PBS. Our strategy, which includes multi-stage optimization and manual intervention, has allowed for the effective control of search space dimension through proper geometry definition. The device produced demonstrates comparable EL and bandwidth performance to conventionally-designed state-of-the-art counterparts, coupled with a significantly more compact footprint. The ER can be improved by cascading the PBSs. In future work, the optimization of our algorithm and structure design could further empower the semi-inverse design method to become even more helpful for device designs.

ACKNOWLEDGMENT

This work was supported by the National Major Research and Development Program (No. 2018YFB2200200); National Science Fund for Distinguished Young Scholars (61725503); National Natural Science Foundation of China (NSFC) (62175216, 61961146003, 91950205); Zhejiang Provincial Natural Science Foundation (LR22F050001); The Fundamental Research Funds for the Central Universities; The Leading Innovative and Entrepreneur Team Introduction Program of Zhejiang (2021R01001).

REFERENCES

[1] D. Dai, "Advanced passive silicon photonic devices with asymmetric waveguide structures," *Proceedings of the IEEE*, vol. 106, no. 12, pp. 2117–2143, 2018.

[2] J. Guo and D. Dai, "Silicon Nanophotonics for on-chip light manipulation," *Chinese Physics B*, vol. 27, no. 10, p. 104208, 2018.

[3] H. Xu, D. Dai, and Y. Shi, "Ultra-Broadband and ultra-compact on-chip silicon polarization beam splitter by using hetero-anisotropic metamaterials," *Laser & Photonics Reviews*, vol. 13, no. 4, p. 1800349, 2019.

[4] J. Guo, L. Yu, H. Xiang, Y. Zhao, C. Liu, and D. Dai, "Realization of advanced passive silicon photonic devices with subwavelength grating structures developed by efficient inverse design," *Advanced Photonics Nexus*, vol. 2, no. 02, 2023.

[5] J. Guo, L. Yu, H. Xiang, Y. Zhao, C. Liu, and D. Dai, "Realization of advanced passive silicon photonic devices with subwavelength grating structures developed by efficient inverse design," *Advanced Photonics Nexus*, vol. 2, no. 02, 2023.

[6] J. Guo, C. Ye, C. Liu, M. Zhang, C. Li, J. Li, Y. Shi, and D. Dai, "Ultra-Compact and ultra-broadband guided-mode exchangers on Silicon," *Laser & Photonics Reviews*, vol. 14, no. 7, p. 2000058, 2020.

[7] Y. Tian, J. Qiu, C. Liu, S. Tian, Z. Huang, and J. Wu, "Compact polarization beam splitter with a high extinction ratio over S + C + L band," Optics Express, vol. 27, no. 2, p. 999, 2019.

[8] H. Xu, D. Dai, and Y. Shi, "Ultra-Broadband and ultra-compact on-chip silicon polarization beam splitter by using hetero-anisotropic metamaterials," Laser & Photonics Reviews, vol. 13, no. 4, p. 1800349, 2019.

[9] H. Xu, D. Dai, and Y. Shi, "Ultra-Broadband and ultra-compact on-chip silicon polarization beam splitter by using hetero-anisotropic metamaterials," Laser & Photonics Reviews, vol. 13, no. 4, p. 1800349, 2019.

[10] L. H. Frandsen and O. Sigmund, "Inverse design engineering of all-silicon polarization beam splitters," SPIE Proceedings, 2016.

[11] W. Chen, B. Zhang, P. Wang, S. Dai, W. Liang, H. Li, Q. Fu, J. Li, Y. Li, T. Dai, H. Yu, and J. Yang, "Ultra-compact and low-loss silicon polarization beam splitter using a particle-swarm-optimized counter-tapered coupler," Optics Express, vol. 28, no. 21, p. 30701, 2020.